

## RESEARCH ARTICLE

# Bmp7 drives proximal tubule expansion and determines nephron number in the developing kidney

Mary Taglienti<sup>1</sup>, Daniel Graf<sup>2</sup>, Valerie Schumacher<sup>1,3,4</sup> and Jordan A. Kreidberg<sup>1,4,5,6,\*</sup>

## ABSTRACT

The mammalian kidney is composed of thousands of nephrons that are formed through reiterative induction of a mesenchymal-to-epithelial transformation by a population of nephron progenitor cells. The number of nephrons in human kidneys ranges from several hundred thousand to nearly a million, and low nephron number has been implicated as a risk factor for kidney disease as an adult. Bmp7 is among a small number of growth factors required to support the proliferation and self-renewal of nephron progenitor cells, in a process that will largely determine the final nephron number. Once induced, each nephron begins as a simple tubule that undergoes extensive proliferation and segmental differentiation. Bmp7 is expressed both by nephron progenitor cells and the ureteric bud derivative branches that induce new nephrons. Here, we show that, in mice, Bmp7 expressed by progenitor cells has a major role in determining nephron number; nephron number is reduced to one tenth its normal value in its absence. Postnatally, Bmp7 also drives proliferation of the proximal tubule cells, and these ultimately constitute the largest segment of the nephron. Bmp7 appears to act through Smad 1,5,9(8), p38 and JNK MAP kinase. In the absence of Bmp7, nephrons undergo a hypertrophic process that involves p38. Following a global inactivation of *Bmp7*, we also see evidence for Bmp7-driven growth of the nephron postnatally. Thus, we identify a role for Bmp7 in supporting the progenitor population and driving expansion of nephrons to produce a mature kidney.

**KEY WORDS:** BMP7, SMAD, Kidney development, Nephron progenitor cell, Proximal tubule, Mouse

## INTRODUCTION

Nephron progenitor cells (NPCs) are a stem-like population in the mammalian kidney that both self-renew and differentiate through a complex process to ultimately form the functional filtration units of the kidney known as nephrons. The human kidney has several hundred thousand to nearly one million nephrons, and the mouse kidney ~15,000 nephrons. The ultimate nephron number obtained during the development of the kidney is important because of increasing evidence that humans at the lower end of the spectrum for

nephron number may be predisposed to kidney disease as adults (Douglas-Denton et al., 2006; Hoy et al., 2008). Furthermore, the mature mammalian kidney does not contain a stem cell population able to replenish nephrons irreversibly damaged by various pathological processes. The self-renewal and proliferation of NPCs is supported by several growth factors, including BMP7, FGF9 and FGF20 (Barak et al., 2012; Dudley et al., 1995; Luo et al., 1995). These are produced both autogenously and by the adjacent ureteric bud derivative branches. The latter are formed from branching morphogenesis originating from the initial ureteric bud that grows out from the Wolffian duct at the caudal end of the urogenital ridge. The self-renewal versus differentiation choice of NPCs is also influenced by Wnt signaling, as Wnt9b from the ureteric bud induces the NPCs to form pretubular aggregates (PTAs), which are transit-amplifying structures that are subsequently induced to undergo a mesenchymal-to-epithelial transformation (MET) by autogenously produced Wnt4 (Carroll et al., 2005; Stark et al., 1994). Once a sufficient number of nephrons are obtained, occurring in human fetuses during gestation and in murine embryos by about postnatal day (P) 2, NPCs disappear from the mammalian kidney and no additional nephrons may be induced (Ryan et al., 2018; Short et al., 2014).

In mice carrying a null mutation of *Bmp7*, there is early demise of NPCs early in kidney development and only a small number of nephrons are induced (Dudley et al., 1995; Luo et al., 1995). A similar phenotype is present in mice carrying double mutations of *Fgf9* and *20* (Barak et al., 2012). The role of Bmp7 signaling in nephrogenesis has been investigated in detail and there is evidence that it signals through both the canonical SMAD pathway and also through JNK and p38 MAP kinases (Blank et al., 2009, 2008; Brown et al., 2013; Hu et al., 2004; Kazama et al., 2008). Bmp7-dependent signaling through JNK MAP kinase may be most important for the self-renewal versus differentiation decision in NPCs, whereas p38 and SMAD-dependent signals may be more involved in nephron differentiation and proliferation (Blank et al., 2009, 2008; Brown et al., 2013; Kazama et al., 2008). However, questions still remain regarding how BMP and FGF signals are integrated in the developing kidney. One possibility is that they contribute to maintaining expression of transcription factors such as SIX2, WT1, EYA1 and others that regulate self-renewal, proliferation and renewal decisions of NPCs (Kopan et al., 2014).

Less well understood is whether there are distinct signaling pathways that maintain progenitor cells as the embryonic kidney expands, and the signals that drive later stages of nephron differentiation and postnatal nephron expansion. It is also unknown whether there are signal transduction events that help maintain nephrons once they are mature. Nephron formation is a complex process that begins with the formation of a simple polarized epithelial structure, the renal vesicle, which then begins a process of segmentation, extension and acquisition of a highly asymmetric three-dimensional structure. During this process there is extensive proliferation and differentiation into many specialized

<sup>1</sup>Department of Urology, Harvard Medical School, Boston, MA 02115, USA. <sup>2</sup>School of Dentistry and Department of Medical Genetics, Faculty of Medicine and Dentistry, University of Alberta, Edmonton, AB T6G 2R7, Canada. <sup>3</sup>Division of Nephrology, Boston Children's Hospital, Harvard Medical School, Boston, MA 02115, USA. <sup>4</sup>Departments of Pediatrics, Harvard Medical School, Boston, MA 02115, USA. <sup>5</sup>Department of Surgery, Harvard Medical School, Boston, MA 02115, USA. <sup>6</sup>Harvard Stem Cell Institute, Cambridge, MA 02139, USA.

\*Author for correspondence (jordan.kreidberg@childrens.harvard.edu)

DOI: 10.1242/dev.200773; M.T., 0000-0002-0428-2717; D.G., 0000-0003-1163-8117; V.S., 0000-0001-8670-0486; J.A.K., 0000-0002-9085-2420

Handling Editor: Liz Robertson

Received 18 March 2022; Accepted 23 June 2022

epithelial cells that carry out filtration in the glomerulus and the homeostatic functions that maintain fluid and electrolyte balance in the tubular segments of the nephron. Several studies have suggested that *Bmp7* is expressed in various segments of the developing and mature nephron, but these studies have obtained varying results, in part because of the difficulty inherent in antibody staining of diffusible growth factors (Wetzel et al., 2006).

We previously published a podocyte-specific knockout of *Bmp7* (Kazama et al., 2008). Loss of *Bmp7* in podocytes resulted in decreased proliferation in the developing nephron and early loss of NPCs, suggesting regulatory crosstalk between the developing nephrons and the NPCs that give rise to them. In the present study, we targeted a mutation to *Bmp7* in NPCs, such that *Bmp7* could not be produced by NPCs or their descendant nephrons (although it could still be produced by derivatives of the ureteric buds, a major source of *Bmp7* during nephrogenesis (Godin et al., 1998)). We observed early loss of progenitors and decreased induction of nascent nephrons during embryonic kidney development. We also observed decreased proliferation in the proximal tubule compartment, although there was hypertrophy of those nephrons that were induced in mutant mice. In addition, we performed a postnatal global inactivation of the *Bmp7* gene that resulted in decreased expansion of the proximal tubule compartment. Therefore, although previous studies have demonstrated a crucial role for *Bmp7* in the self-renewal and differentiation of NPCs at the early stages of kidney development (Blank et al., 2009, 2008; Kazama et al., 2008), this study demonstrates a role for *Bmp7* throughout kidney development, including a role in driving expansion of developing nephrons during postnatal development.

## RESULTS

*Bmp7* is expressed by NPCs, the ureteric bud and segments of the developing nephron (Godin et al., 1998). Therefore, it becomes important to understand whether *Bmp7* produced by NPCs themselves (as opposed to the ureteric bud) and their descendant cell lineages in nephrons plays a major role in nephrogenesis and maintenance of mature nephrons, especially once the ureteric bud derivatives are no longer present. To determine the significance of *BMP7* produced by the NPC compartment or its descendant nephrons to nephrogenesis, we targeted a mutation to the *Bmp7* gene in NPCs using a previously reported BAC *Six2-GFP/Cre* transgene (hereafter referred to as *Six2-TGC*) (Kobayashi et al., 2008) that was crossed with mice carrying a conditional allele of *Bmp7* (Zouvelou et al., 2009) to obtain *Six2-TGC; Bmp7 flox/flox* mice (hereafter referred to as *Bmp7* mutants, and their respective kidneys as *Bmp7* mutant kidneys). *Bmp7* mutant mice were viable and born at normal Mendelian ratios, but became runted by P10 and few survived beyond P25.

### Nephron number and histology in *Bmp7* mutant kidneys

Our initial histological analysis focused on embryonic day (E) 14 and E16 kidneys, by which time a discrete nephrogenic zone has been established. A diminution in kidney size, quantified by measuring the cross-sectional area at the widest diameter of the kidney, was readily apparent in *Bmp7* mutant kidneys by E16.5 (Fig. 1A,B; Fig. S1A,B,F,G). *Six2*-expressing NPCs were not significantly reduced at E14.5, but by E16.5 their reduction was significant (Fig. 1A,C; Fig. S2). Branching morphogenesis in the kidney is primarily driven by GDNF expressed by NPCs. The number of ureteric bud tips was quantified as a measure of branching and was found to also be reduced in *Bmp7* mutant kidneys (Fig. 1D; Fig. S2).

In the murine kidney, NPCs are typically no longer present (or nearly so) after P2, and are completely absent from the adult kidney (Cebrián et al., 2004; Short et al., 2014). Nevertheless, there is tremendous postnatal growth through proliferative expansion of the tubular compartments. Therefore, we examined the postnatal phenotype of *Bmp7* mutant kidneys at successive stages of development. At P2 there are abundant renal vesicles in controls, and fewer immature differentiating structures in *Bmp7* mutants (Fig. S1C,H, green arrows). Histological analysis at successive stages suggests that, at P2 and later stages, the cortex is no longer growing in *Bmp7* mutants (compare Fig. S1C-E with H-K). We also examined kidneys at P21, by which time there are cystic changes in *Bmp7* mutants, evidence of proteinuria and glomerular hypertrophy (Fig. S1K), providing further evidence for the importance of *Bmp7* in maintaining normal kidney structure. Using glomerular counts to enumerate numbers of maturing nephrons, it was apparent that there was a major deficit in nephron number in *Bmp7* mutant kidneys (Fig. 1E). At E16.5, *Bmp7* mutants had only about one third as many glomeruli as controls, and by P2 about a tenth as many (Fig. 1E). These data emphasize the previously documented tremendous expansion of nephron number in postnatal murine kidneys (Cebrián et al., 2004; Short et al., 2014), and demonstrate an early cessation of nephron induction in *Bmp7* mutant kidneys. Consistent with the early loss of NPCs, there was a nearly complete absence of Ki67 staining in the nephrogenic zone of P0 *Bmp7* mutant kidneys (Fig. 2Aa,b), as evidence of greatly reduced proliferation of NPCs.

### Expression of *Bmp7* in embryonic and postnatal kidneys

It is well established that *Bmp7* is expressed by the ureteric bud derivatives in the nephrogenic zone and by NPCs themselves, as well as by immature podocytes (Blank et al., 2009, 2008; Kazama et al., 2008) (Fig. 3Aa). In this study we also observed *Bmp7* expression at P2 and P4 throughout the maturing nephrons of the kidney cortex (Fig. 3Ab-Ac, compare with Af,Ag). Expression by proximal tubules was detected by co-imaging for *Bmp7* mRNA and *Lotus tetragonolobus* lectin (LTL) (Fig. S3). Expression was reduced by P10 (Fig. 3Ad,Ah). Outside of the nephrogenic zone, it has historically been more difficult to determine the expression pattern of *Bmp7*, as lower levels of expression are difficult to distinguish from background hybridization signals. Therefore, it was useful to observe the nearly complete absence of *Bmp7* in mutant kidneys by mRNA *in situ* hybridization (ISH) at E16.5, P2 and P4, except in rare collecting ducts and ureteric bud structures (Fig. 3Ae-Ah). This served to demonstrate not only that our conditional knockout was highly efficient, but also that the hybridization signal outside the nephrogenic zone in control kidneys (Fig. 3Ab-Ad), albeit weaker, was likely to be evidence of continued *Bmp7* expression. *Bmp7* expression detected by RT-qPCR at P2 was also much greater in control versus *Bmp7* mutant kidney cortex (Fig. 3B), confirming differences detected by ISH. In addition, the absence of *Bmp7* expression in most collecting duct structures in mutant kidneys suggests that gene expression in collecting ducts is non-cell autonomously affected by *Bmp7* expression in NPC-derived lineages.

### Gene expression during nephron differentiation in *Bmp7* mutant kidneys

The greatly diminished nephron number in *Bmp7* mutants suggested an early cessation of nephrogenesis. We focused our further analysis on P2 kidneys, because the histology indicated that nephrogenic

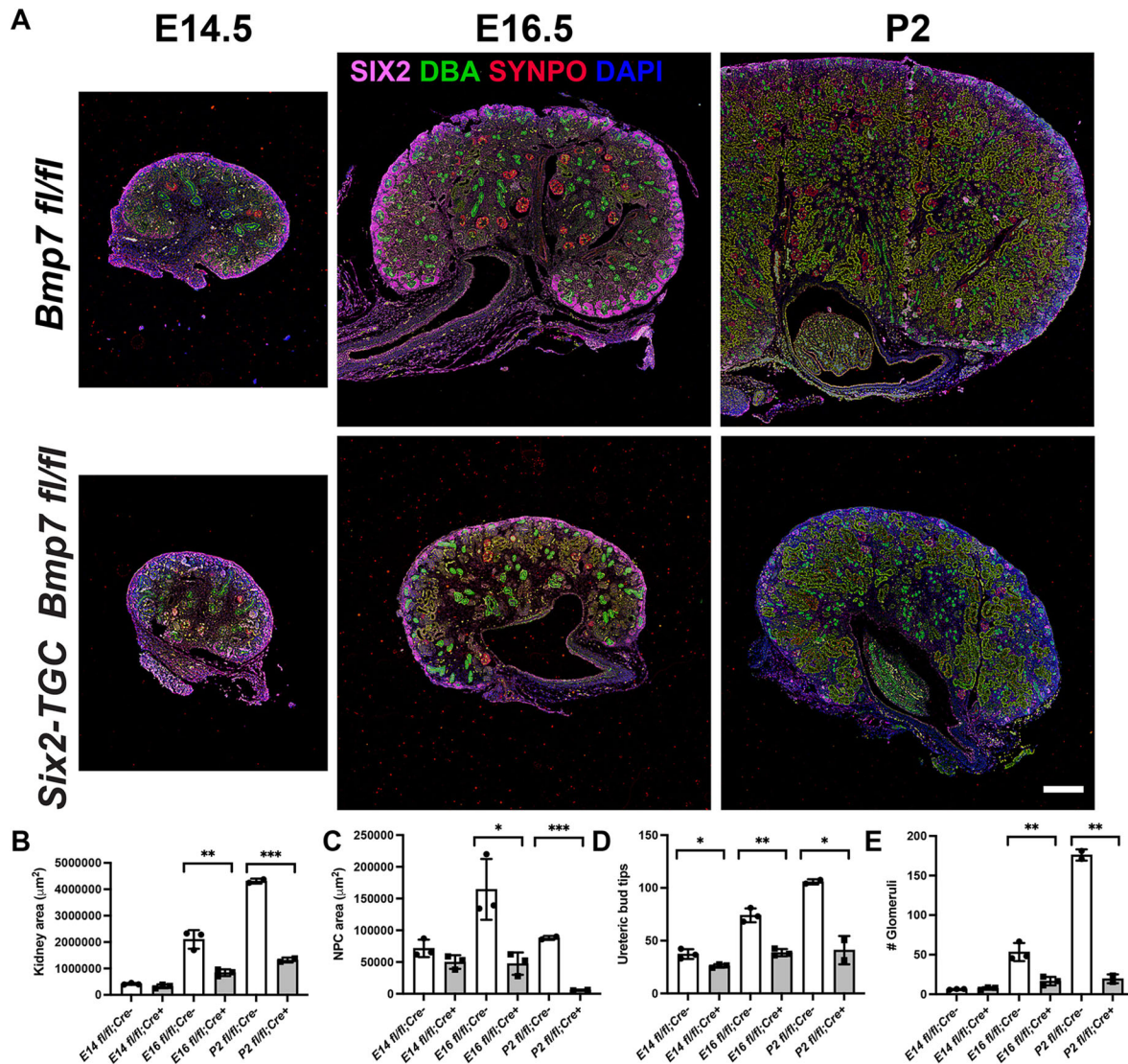


**Fig. 1. NPCs and ureteric bud branching in *Bmp7* mutant kidneys.** (A) Time points at top of each column, genotypes at left of each row. Pink, Six2; green, DBA lectin; red, synaptopodin. The olive-green color in the E16.5 and P2 panels is autofluorescence characteristic of kidney tubules in paraffin-embedded tissues. Scale bar: 250  $\mu\text{m}$ . (B) Cross-sectional kidney area measured at equivalent sections through the papilla at the widest diameter of the kidney. (C) NPC area measured by AF647 fluorescence. (D) Ureteric bud tips measured by counting green-stained tips within clusters of NPCs. (E) Glomerular number obtained by counting structures stained for synaptopodin. Data are mean  $\pm$  s.d. \* $P < 0.05$ , \*\* $P < 0.01$ , \*\*\* $P < 0.001$  (unpaired two-tailed *t*-test). Three biological replicate kidneys were examined at each time point.

structures were diminished but still present in *Bmp7* mutant kidneys. *Pax2*, in a pattern similar to *Bmp7*, is expressed by both ureteric bud derived structures, including the inducing buds themselves and collecting ducts (Fig. 4A, green and yellow arrows), as well as by NPCs and early differentiating nephrons (Armstrong et al., 1993; Dressler et al., 1990; Little et al., 1999) (Fig. 4A, red arrows). *Pax2* expression was present in the few ureteric bud structures remaining in *Bmp7* mutant kidneys but was largely absent in nephron structures (Fig. 4E). *Pax2* expression was preserved in the collecting ducts of mutant kidneys, serving as an internal positive control (Fig. 4E, green arrows). In contrast to *Pax2*, Wilms tumor 1 (*Wt1*) is normally only expressed in NPCs and their descendant structures, most prominently in glomerular podocytes (Armstrong et al., 1993; Little et al., 1999) (Fig. 4B, yellow arrows). *Wt1* was largely absent in *Bmp7* mutant kidneys, even relative to *Pax2* in the nephrogenic zone (Fig. 4F, yellow arrows), suggesting that *Bmp7*-dependent signals dramatically affect expression levels of

key transcription factors in the nephrogenic zone. Moreover, *Wt1* expression was reduced even in the glomeruli that were present in *Bmp7* mutants. Finally, *Wnt4* was examined as a marker of PTAs and renal vesicles (Stark et al., 1994) (Fig. 4C, yellow arrows). *Wnt4* expression was absent in the cortex of P2 mutant kidneys (compare Fig. 4C,D with G,H, with the papillary expression serving as an internal positive control, Fig. 4D,H). The complete absence of *Wnt4*-expressing structures in mutant kidneys is striking as histological analysis showed small areas of differentiating structures present (Fig. S1H, green arrow). Thus, *Bmp7* appears to have a profound effect on the expression of several genes vital to nephron differentiation.

#### Differentiation of loops of Henle and distal tubules

To assess the requirement for *Bmp7* in differentiation of other segments of the nephron, distal tubules and loops of Henle were assessed by staining P2 kidneys for SLC12A3 and SLC12A1,

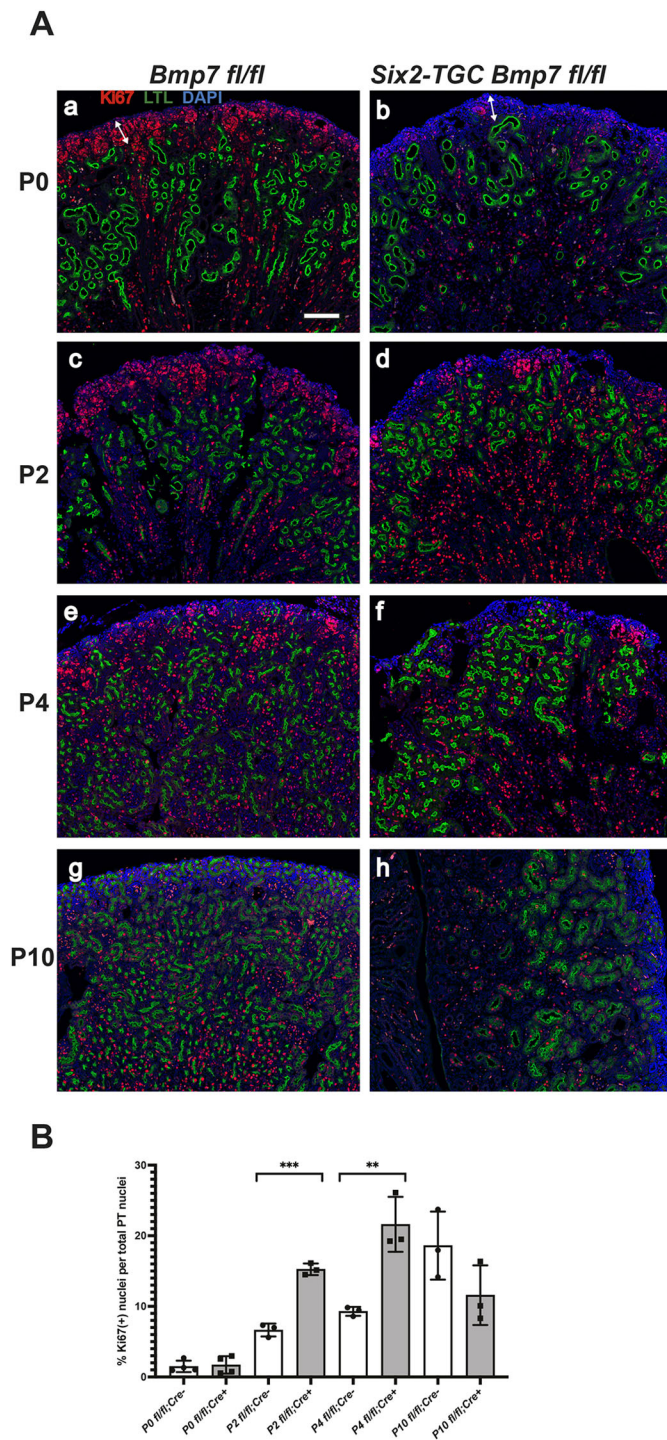


**Fig. 2. Proliferation in proximal tubules.** (A) Sections from P2 kidneys (Aa–Ah) are stained for LTL (green), Ki67 (red) and DAPI (blue). Controls are shown in left column, *Bmp7* mutants in the right column. Postnatal day indicated at left of each row. Double-headed arrows in (Aa, Ab) delimit nephrogenic zone. Scale bar: 100  $\mu$ m. (B) Quantification of Ki67+ nuclei per nuclei of LTL-stained tubules at each time point. Data are mean  $\pm$  s.d. \*\*\* $P < 0.001$ , \*\* $P < 0.01$  (unpaired two-tailed *t*-test). Three biological replicate kidneys were examined at each time point.

respectively (Fig. S4). Both of these ion channels were present in *Bmp7* mutant kidneys, suggesting that epithelial cells of the loops of Henle and distal tubules are able to differentiate in the absence of *Bmp7*.

### Nephron hypertrophy in *Bmp7* mutant kidneys

Despite the great diminution of nephron number in *Bmp7* mutant kidneys, it was evident that they were increasing in size. Therefore, we examined the dynamics of their growth.

Our analysis measured proliferation within the proximal tubule compartment of the nephron, as this ultimately comprises the largest compartment in the adult kidney. Proximal tubule mass was initially quantified by counting numbers of cross sections stained with LTL. This demonstrated a 2.5-fold increase in control kidneys between P0 and P4 (Fig. S5A). However, the number of LTL-stained tubular cross sections in *Bmp7* mutant kidneys was only half that of controls at P0, and increased by less than 50% by P4, such that numbers of cross sections were fivefold greater in controls than in mutants by P4 (Fig. S5A).

Quantifying proximal tubule growth by counting LTL-stained cross sections does not account for the great variation in size of cross sections captured in histological sections. Therefore, to more quantitatively evaluate proximal tubule mass, we computationally measured the area covered by LTL staining at successive time points in the postnatal kidney (Fig. 5A). This approach is useful for comparing control and mutant kidneys at a specific developmental time point. However, proximal tubules at P0 have dilated lumina and those in P4 kidneys are less dilated (Fig. 5C), rendering this computational approach less effective for comparing kidneys across different time points. Nevertheless, this approach also revealed decreased proximal tubule area in *Bmp7* mutants compared with controls at both P0 (Fig. 5Aa) and P4 (Fig. 5Ab). Therefore, both these approaches demonstrate that overall proximal tubule mass is greatly decreased in *Bmp7* mutant kidneys. Staining P2 kidneys for smooth muscle actin demonstrated an increase in interstitial tissue in *Bmp7* mutant kidneys (Fig. S6). Co-staining for Ki67 indicated that there was ongoing proliferation in this interstitial compartment in mutant kidneys.

Although nephrons were much fewer in number in the smaller *Bmp7* mutant kidneys, both approaches to quantifying proximal tubule mass demonstrated that proximal tubule mass per nephron was greater in mutants than in controls at P0 and P4 (Fig. 5Ba and Bb, respectively, and Fig. S5B). Indeed, by P4, proximal tubules measured by area of LTL staining per glomerulus were nearly fivefold higher in *Bmp7* mutant kidneys (Fig. 5Bb). To further understand why proximal tubule mass per nephron was greater in *Bmp7* mutants, we quantified proliferation by counting Ki67-expressing cells within LTL-stained tubules. From P0 through P10, the number of Ki67+ nuclei per LTL+ tubule increased in control kidneys, demonstrating that the proximal tubule compartment is highly proliferative in the early postnatal kidney (Fig. 2A,B). Interestingly, at P2 and P4, Ki67+ nuclei were more abundant per LTL-stained tubule in *Bmp7* mutants compared with control kidneys (Fig. 2Ac–Af,B). By P10, Ki67+ nuclei were still present in *Bmp7* mutants, though by this point less abundant per LTL-stained area than in controls (Fig. 2Ag,Ah,B). These results demonstrate that there is a *Bmp7*-independent compensatory mechanism in mutant hypoplastic kidneys that transiently drives proliferation above normal levels in the proximal tubule compartment.

### BMP7 drives P38 MAPK and SMAD 1,5,9 signaling

BMP signaling during organogenesis drives proliferation and differentiation via two major signal transduction pathways (Feng and Derynck, 2005; Zhang, 2017). A ‘canonical’ pathway uses SMADs 1,5 and 8/9 (Feng and Derynck, 2005). It is also known that BMPs signal through MAP kinase pathways, including those that

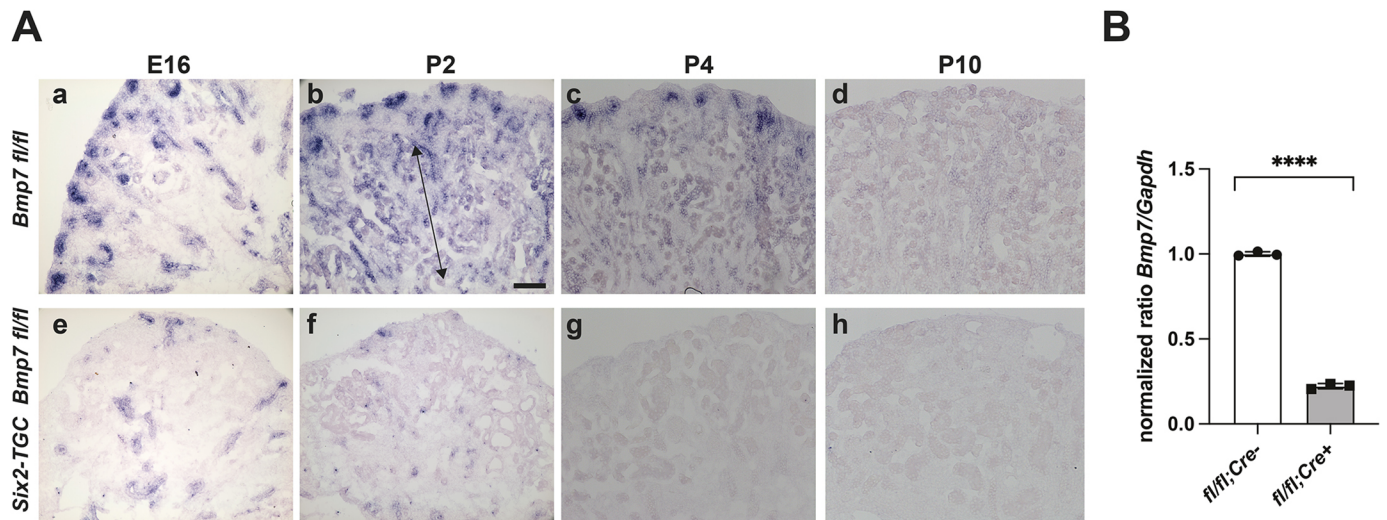


**Fig. 3. *Bmp7* in situ hybridization and RT-qPCR.** (A) *In situ* hybridization of controls (Aa-Ad) and *Bmp7* mutants (Ae-Ah). Embryonic or postnatal day indicated at top of each column. The arrows delimit the region of *Bmp7* expression in maturing nephrons outside the nephrogenic zone. Scale bar: 100  $\mu$ m. (B) RT-qPCR for *Bmp7* in P2 kidneys. Data are mean  $\pm$  s.d. \*\*\*\* $P < 0.0001$  (unpaired two-tailed *t*-test). Three biological replicate kidneys were examined at each time point.

involve p38 and JNK (Zhang, 2017). Previous studies have suggested that the p38 or JNK pathways may be more operative in determining progenitor cell self-renewal versus nephron differentiation and that the SMAD pathway is more involved in nephron differentiation (Blank et al., 2009, 2008; Brown et al., 2013). Detection of phospho-p38 (pp38) at successive time points in postnatal kidneys revealed it to be widely present in the nephrogenic zone and both epithelial and interstitial cells throughout the cortex of control kidneys (Fig. 6Aa,Ac,Ae). At P1, pp38 was largely absent in *Bmp7* mutants (Fig. 6Aa,Ab), suggesting that a p38-dependent signal is indeed a major pathway through which *Bmp7* signals during early postnatal kidney development.

However, by P3 and P7, the abundance of pp38 increased in *Bmp7* mutants, to levels similar to that observed control kidneys (Fig. 6Ac-Af). Interestingly, at P7 pp38 remains prominent in the outermost cortex in both control and mutant kidneys (Fig. 6Ae,Af), further supporting a role for p38-mediated signaling in the maturation of nephrons. There are multiple isoforms of p38, all of which are detected by immunohistological staining with anti-pp38 antibodies. To determine whether there was an isoform shift in *Bmp7* mutants, we performed a western blot for pp38 using tissue from P2 kidneys, a time point at which pp38 is starting to become more prominent in *Bmp7* mutant kidneys. In control kidneys, there appeared to be a single major isoform phosphorylated

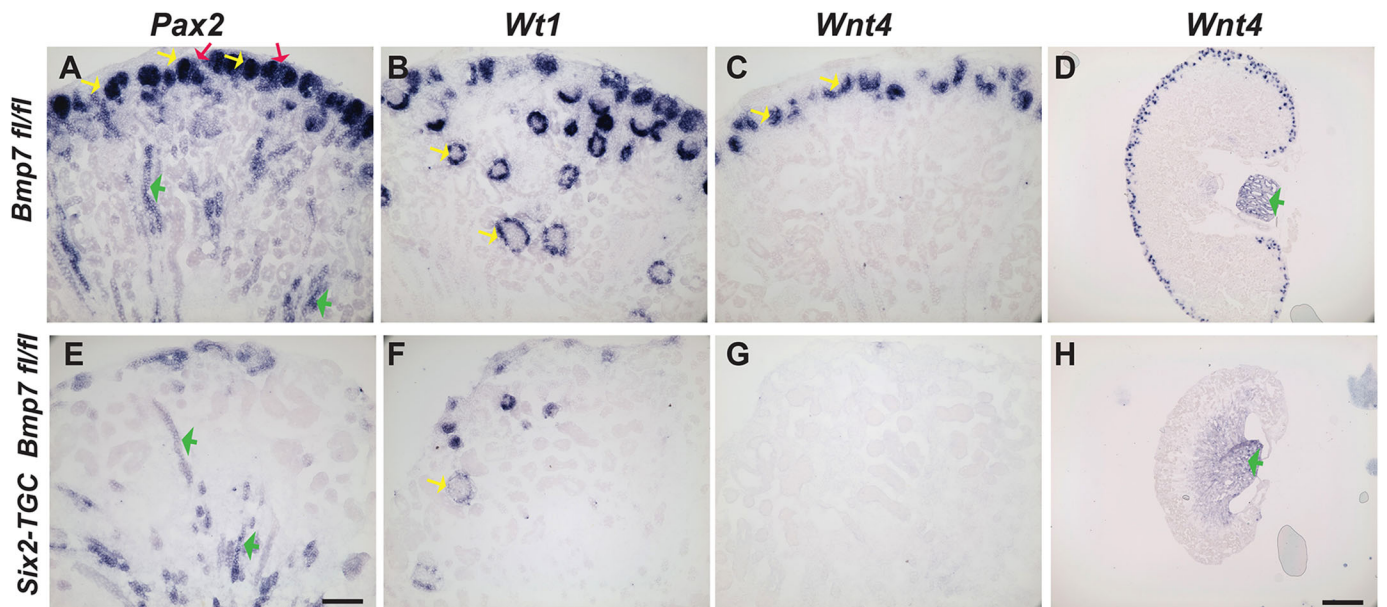


**Fig. 4. Gene expression in control and *Bmp7* mutant P2 kidneys.** (A-H) *In situ* hybridization of controls (A-D) and *Bmp7* mutants (E-H). The gene is indicated at the top of each column. (A,E) Yellow arrows, renal vesicles; red arrows, ureteric bud derivatives; green arrows, collecting ducts. (B,F) Yellow arrows, podocytes in maturing glomeruli. (C) Yellow arrows, renal vesicles. (D,H) Green arrows, *Wnt4* expression in papilla. Scale bars: 100  $\mu$ m (A-C, E-G); 500  $\mu$ m (D, H). Three biological replicate kidneys were examined at each time point.

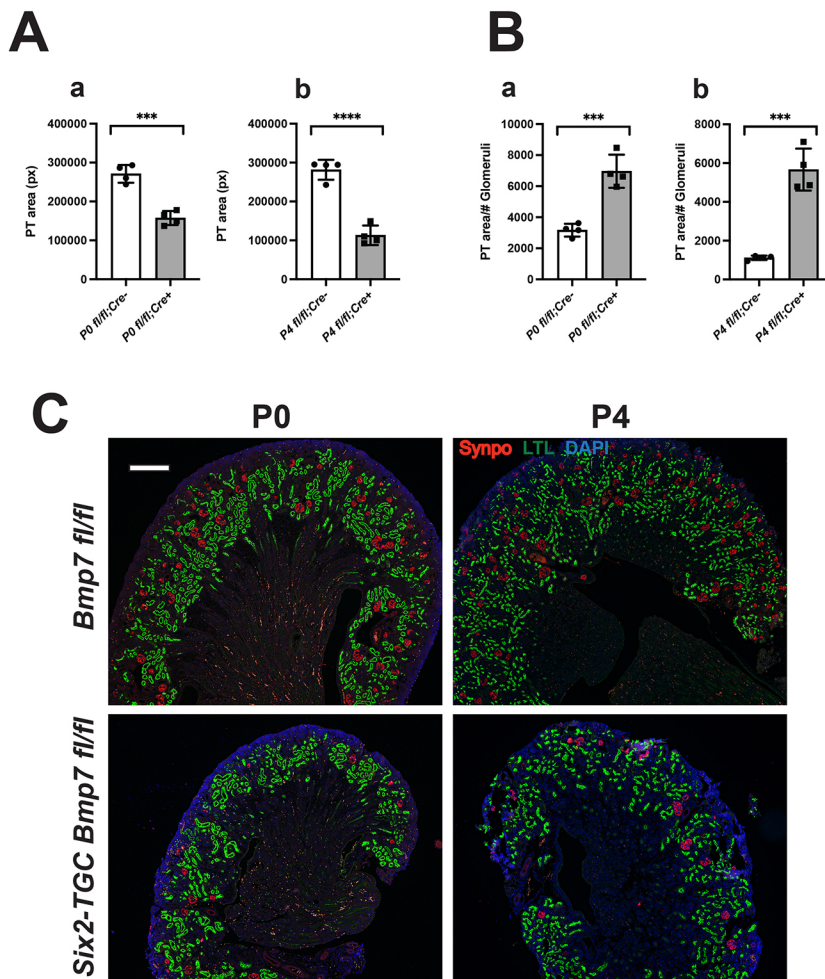


**Fig. 5. Proximal tubule analysis.** (A) Quantification of area of LTL staining in P0 and P4 kidneys by pixel counts in P0 (Aa) and P4 (Ab) kidneys. The P0 and P4 pixel counts cannot be directly compared owing to differences in appearance of the tubules. (B) PT area per glomerulus in P0 (Ba) and P4 (Bb) kidneys. Data are mean $\pm$ s.d. \*\*\*\* $P$ <0.0001, \*\*\* $P$ <0.001 (unpaired two-tailed  $t$ -test). (C) LTL (green) and anti-synaptopodin (red) staining. DAPI: blue. Scale bar: 100  $\mu$ m. Three biological replicate kidneys were examined at each time point.

(Fig. 6B, black arrow). In contrast, two bands with approximately equal stoichiometry were present at 38 kd in *Bmp7* mutant kidneys (Fig. 6B, black and red arrows). This doublet may represent a band-shift of the isoform that predominates in control kidneys or the activation of a second isoform. Although we cannot exclude the possibility that an alternate isoform of p38 mediates the hypertrophic response, the detection of a single band (using an anti-p38 antibody that should detect multiple isoforms), suggests that a single isoform predominates in both control and *Bmp7* mutant kidneys. The amount of total p38 present was lower in *Bmp7* mutants, suggesting that, although present at lower amounts, the proportion of p38 phosphorylated is higher in *Bmp7* mutants. These results suggest that there is both *Bmp7*-dependent and -independent p38 signaling in early postnatal kidney development.

Phospho-SMAD 1,5,8 is also abundant in P2 postnatal kidneys, both in the nephrogenic zone (Fig. 7A, green arrows), including NPCs, capsular and interstitial cells, glomeruli and some tubular epithelial cells. It is also abundant in the medullary region and cortical collecting ducts (Fig. 7A, white arrow). In *Bmp7* mutant kidneys, pSMAD 1,5,9(8) is greatly reduced in the nephrogenic zone and cortical epithelia, but still present in non-NPC-derived lineages including collecting ducts and interstitial cells, as well as in the medullary region (Fig. 7B), consistent with *Bmp7* having been conditionally mutated in NPCs. By P10, pSMAD 1,5,9(8) is most prominent in glomeruli and remains abundant in the medulla of control kidneys, (Fig. 7C, yellow arrows), but is

largely absent in *Bmp7* mutant kidneys (Fig. 7D). These results suggest that *Bmp7* is the most prominent driver of SMAD 1,5,9 signaling in the postnatal kidney. They also suggest that loss of *Bmp7* in NPCs and their descendant cells affects SMAD 1,5,9(8) signaling in the adjacent interstitium.

#### Postnatal role for *Bmp7* in nephron expansion

As previously mentioned, there is tremendous postnatal growth of the kidney. To distinguish the role of *Bmp7* in driving postnatal growth from its role in maintaining NPCs, we inactivated the *Bmp7* gene at P7, when NPCs are no longer present and all nephrons have been induced. A *Rosa26-CreERT2* transgene was used to broadly reduce levels of *Bmp7*, irrespective of its tissue of origin. In the kidney, we were able to achieve a 50% reduction in the level of *Bmp7* mRNA (Fig. 8B). At P7, before inactivation, kidneys of *Bmp7*<sup>fl/fl</sup> and *Bmp7*<sup>fl/fl</sup>; *Rosa26-CreERT2* mice (henceforth R26 *Bmp7* mutants) were identical in all respects (Fig. 8C-H). Reduction of *Bmp7* did not affect the number of glomeruli, suggesting there was not a reduction in nephron number (Fig. 8C). However, at P21, 14 days after inactivation of *Bmp7*, there was a significant decrease in proximal tubule area and cross-sectional area of the kidneys (Fig. 8A,D,E). There was also a decrease (albeit not significant) in body and kidney weight of mutant mice (Fig. 8F,G). Kidney-to-body weight ratios were similar in both control and mutant mice (Fig. 8H). Examination of the activation status of signaling pathways acting downstream of *Bmp7* showed a dramatic loss of pSmad 1,5,9(8) in mutant kidneys, both in

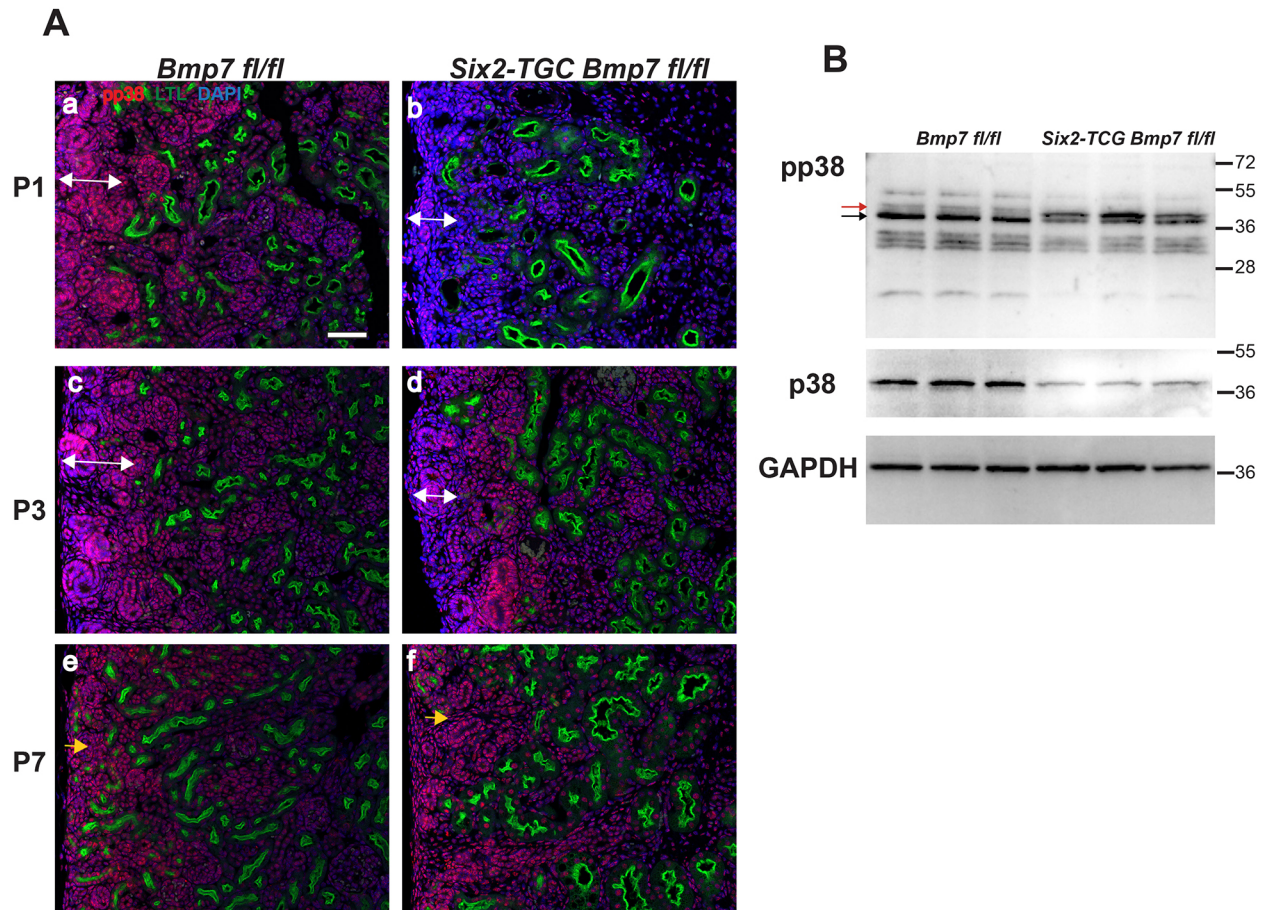


**Fig. 6. (A) Phospho-p38 staining in P2 kidneys.** (A) Sections (Aa-Af) are stained for LTL (green), pp38 (red) and DAPI (blue). Controls are shown in the left column, *Bmp7* mutants in the right column. The double headed arrow delimits the extent of the nephrogenic zone containing immature structures. By P7 the nephrogenic zone has disappeared. Yellow arrows (Ae,Af) indicate areas of pp38 in the more peripheral cortex. Scale bar: 100  $\mu$ m. (B) Western blot for pp38. The black and red arrows indicate the doublet band in the mutant at 38 kd.

proximal tubules and glomeruli (Fig. 9A). In contrast, pp38 was broadly present in the cortical epithelial and interstitial cells of P21 kidneys and was greatly reduced in R26 *Bmp7* mutant

littermates (Fig. 9B). pJNK appeared to be less abundant than pp38 and was generally excluded from LTL+ tubules. pJNK was also diminished in R26 *Bmp7* mutants (Fig. 9C). Thus,

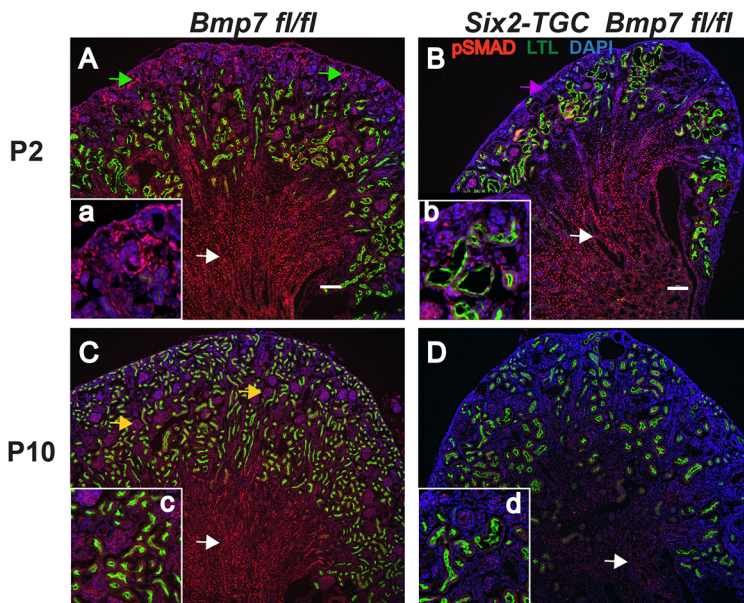


**Fig. 7. Phospho-Smad 1,5,8 staining in P2 kidneys.** (A-D) Sections are stained for LTL (green), pSmad 1,5,8 (red) and DAPI (blue). Green arrow (A) indicates pSMAD present in nascent nephrons. Inset (Aa) shows pSMAD in differentiating tubules. Pink arrow (B) indicates the thin nephrogenic zone without pSMAD present. Inset (Bb) shows the few pSMAD+ cells in immature nephrons. Yellow arrows (C) indicate pSMAD present in glomeruli. Inset (Cc) shows pSMAD in glomeruli. White arrows (C,D) show pSMAD present in collecting ducts of medulla and papilla. Little pSMAD staining is seen in *Bmp7* mutant (D,Dd). Scale bars: 100  $\mu$ m. Three biological replicate kidneys were examined at each time point.

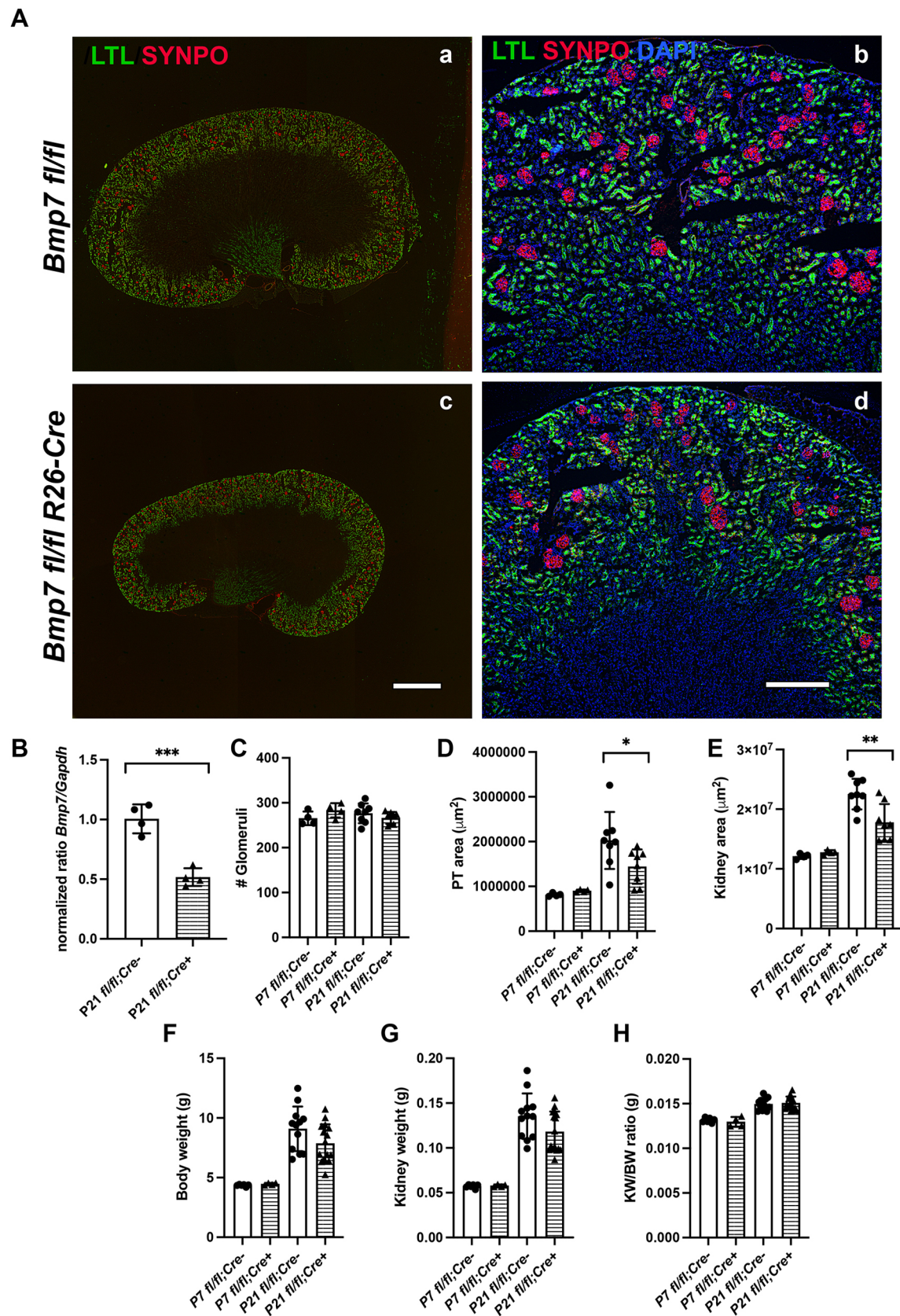


**Fig. 8. Quantification of R26 *Bmp7* mutant kidneys.** (A) Representative LTL/synaptopodin images used for quantification shown in (B-E). Scale bars: 1 mm (Aa,Ac); 250  $\mu\text{m}$  (Ab,Ad). (B-H) All analyses show multiple biological replicates comparing controls and R26 *Bmp7* mutants at P7 and P21. (B) RT-qPCR for *Bmp7* in P21 kidneys. (C) Glomerular quantification. (D) Proximal tubule area based on LTL stain. (E) Kidney cross-sectional diameter at widest diameter section through papilla. (F) Body weight of mice. (G) Kidney weight. (H) Ratio of kidney to body weight. Data are mean  $\pm$  s.d. \*\*\* $P < 0.001$ , \*\* $P < 0.01$ , \* $P < 0.05$  (unpaired two-tailed *t*-test). At least three biological replicate kidneys were examined at each time point.

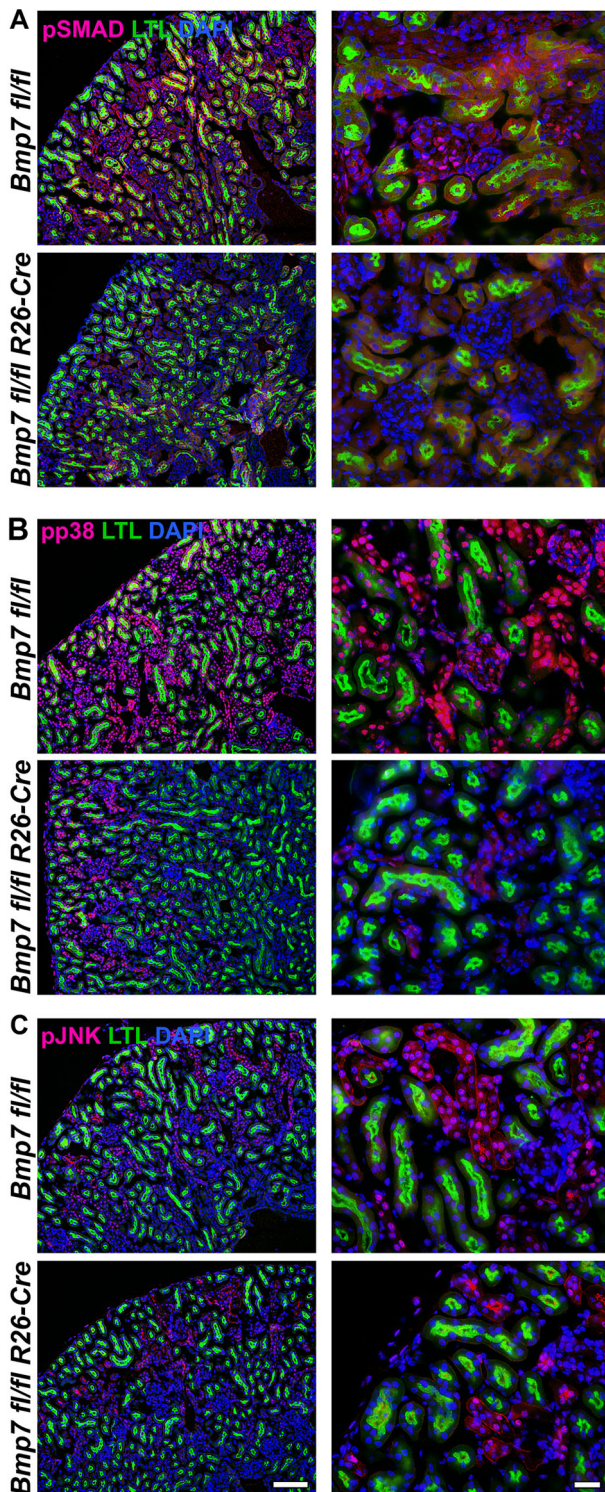


**Fig. 9. pSMAD, pp38 and pJNK localization in R26 *Bmp7* mutants.** (A-C) All panels are from kidneys of P21 mice. Genotypes are shown on the left. A low power (left) and high power (right) field is shown for each analysis. (A) pSMAD 1,5,9 localization. (B) pp38 localization. (C) pJNK localization. All images are representative of three biological replicates. Scale bars: 100  $\mu$ m (left-hand column); 25  $\mu$ m (right-hand column). Three biological replicate kidneys were examined at each time point.

*Bmp7*-dependent signaling, both through Smad 1,5,9(8) and p38 and JNK, remains highly operative during postnatal growth of the kidney.

## DISCUSSION

Several important conclusions about the role of *Bmp7* in the developing and postnatal kidney may be drawn from our results: (1) although the ureteric bud is a major source of *Bmp7* in the embryonic kidney, *Bmp7* expressed by the *Six2*+ derived progenitor population is a crucial determinant of nephron number in the adult kidney; (2) *Bmp7* continues to be expressed in the tubular compartment of the postnatal kidney; (3) *Bmp7* is at least partially responsible for driving expansion of the proximal tubule compartment in the postnatal kidney; (4) there is a *Bmp7*-independent compensatory mechanism driving proliferation in hypertrophic proximal tubules of hypoplastic kidneys; and (5) pSMAD 1,5,9(8) and p38 signaling appears to be largely dependent on *Bmp7* in the nephrogenic zone, whereas an alternate isoform of p38 may mediate the compensatory postnatal response to the absence of *Bmp7*.

The original *Bmp7* null mutant mouse phenotype included greatly hypoplastic kidneys that appeared to have undergone, at most, a single round of nephron induction, after which the remaining progenitors underwent apoptosis, demonstrating a crucial role for *Bmp7* in the self-renewal and proliferation of the progenitor population (Dudley et al., 1995; Luo et al., 1995). By using the *Six2-TGC* transgenic mouse, which expresses Cre recombinase in the *Six2*-expressing cap mesenchyme (Kobayashi et al., 2008), we explored the requirement for *Bmp7* expression specifically from progenitors and their descendant nephron epithelial cells. The phenotype obtained demonstrates that *Bmp7* expressed by ureteric bud-derived tissue is unable to maintain NPCs in the embryonic kidney. Morphometric studies have shown that the majority of the nephrons in the murine kidney are induced during the last two days of embryogenesis and the first two days of postnatal development (Cebrián et al., 2004; Short et al., 2014). This massive expansion of nephron number is completely absent from *Bmp7* mutant mice. At P0 there is an approximately threefold difference in nephron number in *Bmp7* mutants that increases to a tenfold difference by P4, indicating that the deficit in the ability to induce new nephrons is still evolving at P0.

The markedly lower nephron number in *Bmp7* mutant kidneys, as well as their overall architecture, is most consistent with decreased proliferation and self-renewal of progenitor cells after E14.5. As discussed above, there is normally an approximately tenfold increase in nephron number between E16.5 and P2, which largely fails to occur in *Bmp7* mutant kidneys. On the other hand, during normal kidney development there is typically a transition that occurs between E15.5 and E17.5, during which a discrete nephrogenic zone is established in the developing kidney. Although E16.5 *Bmp7* mutant kidneys appear to be considerably less well developed than control kidneys, by P0 the overall architecture of mutant kidneys is grossly correct, with collecting ducts projecting from a medulla to the outermost cortex, and convolutions of proximal and distal tubules in the cortex, underlying a nephrogenic zone containing less differentiated structures. The understanding of how the kidney develops very distinct cortical and medullary zones, as well as the specific patterns found within each zone, is relatively limited. Nevertheless, the histology of *Bmp7* mutant kidneys suggests that the overall architecture of the kidney is determined very early in its formation and does not require continued induction of new nephrons throughout embryogenesis. Moreover, the nephron hypertrophy in *Bmp7* mutants did not cause great distortions in the patterning of the kidney.

The induction and differentiation of nephrons is dependent on crucial reciprocal inductive interactions between the ureteric bud

and the progenitor population. Most notably, *Wnt9b* expressed by the ureteric bud induces the formation of PTAs, and *GDNF* expressed by progenitors induces growth and branching of the ureteric bud and its derivative branches (Carroll et al., 2005). *Bmp7* is expressed by both the ureteric bud and progenitor compartments (Oxburgh et al., 2011; Oxburgh and Robertson, 2002). Both sources of *Bmp7* appear to be vital to achieve the full developmental potential of the kidney. Unexpectedly, as shown by the *Bmp7* ISH in Fig. 3Ae, Af, *Bmp7* expression in *Bmp7* mutant kidneys is not only decreased in the progenitor and nephron compartments, but also in ureteric bud-derived structures at E16.5 and P2. This suggests that *Bmp7* expression in ureteric bud-derived structures may be non-autonomously affected by *Bmp7* expression in progenitors in developing nephrons. In addition, greatly decreased *Pax2* and *Wnt4* expression in *Bmp7* mutant kidneys also suggests that gene expression is affected not only in developing nephrons but also non-autonomously in ureteric bud derivatives and collecting ducts. Together, these results suggest that the reciprocal interactions between progenitor/nephron compartments and the ureteric bud-derived compartments may be more profound than previously recognized.

### Nephron hypertrophy

The phenotype described here bears resemblance to the condition of oligomeganephronia in humans. This is a rare condition described as over 80% reduction in nephron number, accompanied by hypertrophy of glomeruli and tubules (Carter and Lirenman, 1970). Oligomeganephronia has been observed as a component of several syndromes, including Renal Coloboma syndrome and Wolf-Hirschhorn syndrome (Gatto et al., 2018; Park and Chi, 1993; Salomon et al., 2001). As the former is caused by mutations in the *Pax2* gene, it is interesting that *Pax2* expression is greatly reduced in kidneys of *Bmp7* mutant mice. However, *Bmp7* appears to be expressed more broadly in the developing nephrons than *Pax2*, which is predominantly expressed in the cap mesenchyme and renal vesicles, whereas we observe broad *Bmp7* expression in much of the developing cortex. Therefore, although *Bmp7* may help maintain *Pax2* expression in the early nephron, *Bmp7* may drive subsequent proximal tubule expansion independently of *Pax2*. The etiology for the hypertrophy in oligomeganephronia is not well understood. However, our results suggest that it may involve activation of a p38 MAP kinase-mediated pathway.

### Postnatal role for *Bmp7*

The reduction in pSmad 1,5,9(8) observed after constitutive inactivation of *Bmp7* provides evidence of a role for *Bmp7* in the differentiation and early growth of the nephron. However, the nephron hypertrophy observed in these kidneys obscured whether *Bmp7* drives nephron expansion. This issue was addressed by performing a postnatal inactivation of *Bmp7*. Cross-sectional areas of R26 *Bmp7* mutant kidneys were reduced, as was pSMAD1,5,9(8) and pJNK staining, all consistent with a direct role for *Bmp7* in postnatal expansion of the proximal tubule compartment. However, the broad inactivation of *Bmp7* led to some degree of decreased growth of R26 *Bmp7* mutant mice, such that kidney-to-body weight ratios were unchanged. Therefore, although we cannot exclude the possibility that reduction in kidney size is secondary to an overall growth deficit resulting from systemic loss of *Bmp7*, the dramatic reduction in pSMAD 1,5,9(8), pp38 and, to a lesser extent, pJNK staining are more consistent with a direct effect of *Bmp7* on the kidney.

## MATERIALS AND METHODS

### Mice

All animal studies were carried out in accordance with the guidance of the Institutional Animal Care and Use Committee at Boston Children's Hospital. *Bmp7* floxed mice were as previously published (Kazama et al., 2008; Zouvelou et al., 2009), and were originally obtained from Dr Aris Economides (Regeneron Corp., NY, USA). BAC transgenic *Six2-TGC* mice (Kobayashi et al., 2008) were obtained from Dr Andrew McMahon (formerly Harvard University, MA, USA). *Rosa26-CreERT2* mice are from The Jackson Laboratory (strain #008463).

### Antibodies and reagents

LTL-fluorescein (Vector Laboratories, #FL-1321, 1:200); DBA-fluorescein (Vector Laboratories, #FL-1031, 1:200); anti-SLC12A1 (Proteintech, #18970-1-AP, 1:400); anti-SLC12A3 (Sigma-Aldrich, #HPA028748, 1:200); anti-synaptopodin (kindly provided by Dr Peter Mundel, Atlas Venture, Cambridge, MA, USA; 1:200); anti-Ki67 (Vector Laboratories, #VP-RM04, 1:150); anti-SMA (Abcam, #ab5694, 1:300); anti-pp38 (Cell Signaling Technology, #4511, 1:100); anti-p38 (Cell Signaling Technology, #9212, 1:100); ProLong Gold Antifade Mountant with DAPI (Thermo Fisher Scientific, #P36931), 1:1 dilution in Fluoro-Gel (Electron Microscopy Sciences, #17985-10); anti-Six2 (Proteintech, #11562-1-AP, 1:250); anti-pSAPK/JNK (Cell Signaling Technology, #9251, 1:100); anti-pSmad 1/5/8 (kindly provided by Dr Malcolm Whitman, Harvard Medical School, MA, USA; 1:80). All secondary antibodies were used at 1:1000 dilution. Goat anti-rabbit IgG (H+L) Alexa Fluor 568 (Thermo Fisher Scientific, #A11036); goat anti-rabbit IgG (H+L) Alexa Fluor +647 (Thermo Fisher Scientific, #A32733); goat anti-mouse IgG1 Alexa Fluor 568 (Thermo Fisher Scientific, #A21124).

### Proximal tubule quantification

Kidney sections were prepared in paraffin and stained with LTL-fluorescein and anti-synaptopodin to visualize proximal tubules and glomeruli, respectively. Using NIS-Elements AR software (Nikon), the area of LTL staining was quantified as the number of green pixels detected. Intensity and area thresholds were set to remove background signals or areas not representative of proximal tubules, based on area, diameter, circularity and location within the kidney. Using these settings as a basis for defining proximal tubule cross sections, numbers of such structures were counted per section using the software. Numbers of glomeruli were counted manually using a software assist for tallying purposes. Data are presented both as area of green pixels (LTL area) per glomerulus and number of proximal tubule cross sections per glomerulus. For each time point, at least three control and mutant biological replicate sections were examined.

### Glomerular counts

Numbers of glomeruli were quantified by counting total glomeruli in a single longitudinal histological section from the widest diameter of the kidney. For each time point, at least three kidneys from littermate individual mice were analyzed.

### Immunohistochemistry

All Figures were prepared using paraffin-embedded sections except for pSMAD 1,5,8 and SLC12A1, SLC12A3. For staining of paraffin-embedded sections, after removal of paraffin, sections were treated with citrate buffer for antigen retrieval, permeabilized with 0.025% Triton X-100 in Tris buffered saline (TBS) for 10 min at room temperature and blocked with 10% goat serum and 1% bovine serum albumin (BSA) for 2 h at room temperature. Sections were incubated with primary antibodies with 1:200-1:1000 dilution in 1% BSA in TBS at 4°C overnight, then incubated in secondary antibody (Alexa Fluor) at 1:1000 dilution in 1% BSA in TBS at room temperature for 1 h and mounted with anti-fade reagent as above. Kidneys were fixed with 4% paraformaldehyde/PBS overnight at 4°C, cryoprotected in 30% sucrose/PBS overnight at 4°C, and then embedded/frozen in OCT. Immunofluorescence staining carried out on kidney cryosections (6 µm, Leica CM3050S) were counterstained with Prolong Gold Antifade Mountant with DAPI.

## RNA ISH

Kidneys were fixed in 4% paraformaldehyde in DEPC-treated PBS overnight, cryoprotected in 30% sucrose/PBS overnight at 4°C, and then embedded in OCT. We prepared 10 µm cryosections (Leica CM3050S) for RNA ISH (as previously described; Kann et al., 2015). Probes have been previously described (Hartwig et al., 2010; Kann et al., 2015). ISH probes were prepared using the PureLink Plasmid Maxiprep Kit (Thermo Fisher Scientific, #K210017) for plasmid isolation. Purification of linearized plasmids was performed using the Qiagen MinElute PCR Purification Kit (#28004). All restriction enzymes for plasmid linearizations were from New England Biolabs. Synthesis of DIG-labeled RNA probes was performed with the SP6/T7 Transcription Kit from Roche (#10999644001). Non-incorporated nucleotides were removed using the Roche mini Quick Spin RNA columns (#11814427001). Probe development and detection was performed using anti-DIG-AP Fab fragments, Roche (#11093274910) and BM Purple AP Substrate, Roche (#11442074001).

## RT-qPCR

cDNA synthesis was carried out using SuperScript III first strand synthesis system (Thermo Fisher Scientific, #18080051) and RT-qPCR was performed using a SYBR Green PCR Master Mix (Thermo Fisher Scientific, #4364346) and run on a QuantStudio 3 RT-PCR system (Applied Biosystems). Primer pairs have been previously described (Hartwig et al., 2010; Kann et al., 2015). The kidney cortex was microdissected apart from the medullary region before preparation of mRNA. The forward primer was ACGGACAGGCTTCTCC-TAC; the reverse primer was ATGGTGGTATCGAGGGTGGAA. The primers are in exon 1 and 2 and do not detect a *Bmp7* mRNA product from the mutant allele (Zouvelou et al., 2009).

## Statistics

All data are presented as mean±s.d. and calculations were performed using Microsoft Excel. Unpaired one-tailed Student's *t*-test was used for glomerular counts and unpaired two-tailed Student's *t*-test was used for all other data to determine statistical significance. *P*-value <0.05 was considered to be statistically significant.

## Acknowledgements

We thank Drs Aris Economides (Regeneron Corporation) for the gift of the *Bmp7* floxed mice, Malcolm Whitman (Harvard Medical School) for providing the anti-pSMAD antibody and Dr Seymour Rosen (Beth Israel Deaconess Medical Center) for valuable discussions.

## Competing interests

The authors declare no competing or financial interests.

## Author contributions

Conceptualization: M.T., V.S., J.A.K.; Methodology: M.T.; Formal analysis: J.A.K.; Investigation: M.T., V.S.; Resources: D.G.; Writing - original draft: M.T., J.A.K.; Writing - review & editing: M.T., D.G., V.S., J.A.K.; Visualization: M.T.; Supervision: J.A.K.; Project administration: J.A.K.; Funding acquisition: J.A.K.

## Funding

This research was funded by the National Institutes of Health (5R01DK087794 to J.A.K.). Deposited in PMC for release after 12 months.

## References

- Armstrong, J. F., Pritchard-Jones, K., Bickmore, W. A., Hastie, N. D. and Bard, J. B. (1993). The expression of the Wilms' tumour gene, WT1, in the developing mammalian embryo. *Mech. Dev.* **40**, 85-97. doi:10.1016/0925-4773(93)90090-K
- Barak, H., Huh, S. H., Chen, S., Jeanpierre, C., Martinovic, J., Parisot, M., Bole-Feyssot, C., Nitschke, P., Salomon, R., Antignac, C. et al. (2012). FGF9 and FGF20 maintain the stemness of nephron progenitors in mice and man. *Dev. Cell* **22**, 1191-1207. doi:10.1016/j.devcel.2012.04.018
- Blank, U., Seto, M. L., Adams, D. C., Wojchowski, D. M., Karolak, M. J. and Oxburgh, L. (2008). An in vivo reporter of BMP signaling in organogenesis reveals targets in the developing kidney. *BMC Dev. Biol.* **8**, 86. doi:10.1186/1471-213X-8-86
- Blank, U., Brown, A., Adams, D. C., Karolak, M. J. and Oxburgh, L. (2009). BMP7 promotes proliferation of nephron progenitor cells via a JNK-dependent mechanism. *Development* **136**, 3557-3566. doi:10.1242/dev.036335
- Brown, A. C., Muthukrishnan, S. D., Guay, J. A., Adams, D. C., Schafer, D. A., Fetting, J. L. and Oxburgh, L. (2013). Role for compartmentalization in nephron progenitor differentiation. *Proc. Natl. Acad. Sci. USA* **110**, 4640-4645. doi:10.1073/pnas.1213971110
- Carroll, T. J., Park, J. S., Hayashi, S., Majumdar, A. and McMahon, A. P. (2005). Wnt9b plays a central role in the regulation of mesenchymal to epithelial transitions underlying organogenesis of the mammalian urogenital system. *Dev. Cell* **9**, 283-292. doi:10.1016/j.devcel.2005.05.016
- Carter, J. E. and Lirenman, D. S. (1970). Bilateral renal hypoplasia with oligomeganephronia. Oligomeganephronic renal hypoplasia. *Am. J. Dis. Child.* **120**, 537-542. doi:10.1001/archpedi.1970.02100110085009
- Cebrián, C., Borodo, K., Charles, N. and Herzlinger, D. A. (2004). Morphometric index of the developing murine kidney. *Dev. Dyn.* **231**, 601-608. doi:10.1002/dvdy.20143
- Douglas-Denton, R. N., McNamara, B. J., Hoy, W. E., Hughson, M. D. and Bertram, J. F. (2006). Does nephron number matter in the development of kidney disease? *Ethn. Dis.* **16**, S2-40-45.
- Dressler, G. R., Deutsch, U., Chowdhury, K., Nornes, H. O. and Gruss, P. (1990). Pax2, a new murine paired-box-containing gene and its expression in the developing excretory system. *Development* **109**, 787-795. doi:10.1242/dev.109.4.787
- Dudley, A. T., Lyons, K. M. and Robertson, E. J. (1995). A requirement for bone morphogenetic protein-7 during development of the mammalian kidney and eye. *Genes Dev.* **9**, 2795-2807. doi:10.1101/gad.9.22.2795
- Feng, X.-H. and Derynck, R. (2005). Specificity and versatility in TGF-β signaling through Smads. *Annu. Rev. Cell Dev. Biol.* **21**, 659-693. doi:10.1146/annurev.cellbio.21.022404.142018
- Gatto, A., Ferrara, P., Leoni, C., Onesimo, R., Zollino, M., Emma, F. and Zampino, G. (2018). Oligonephronia and Wolf-Hirschhorn syndrome: a further observation. *Am. J. Med. Genet. A* **176**, 409-414. doi:10.1002/ajmg.a.38554
- Godin, R. E., Takaesu, N. T., Robertson, E. J. and Dudley, A. T. (1998). Regulation of BMP7 expression during kidney development. *Development* **125**, 3473-3482. doi:10.1242/dev.125.17.3473
- Hartwig, S., Ho, J., Pandey, P., Macisaac, K., Taglienti, M., Xiang, M., Alterovitz, G., Ramoni, M., Fraenkel, E. and Kreidberg, J. A. (2010). Genomic characterization of Wilms' tumor suppressor 1 targets in nephron progenitor cells during kidney development. *Development* **137**, 1189-1203. doi:10.1242/dev.045732
- Hoy, W. E., Bertram, J. F., Denton, R. D., Zimanyi, M., Samuel, T. and Hughson, M. D. (2008). Nephron number, glomerular volume, renal disease and hypertension. *Curr. Opin. Nephrol. Hypertens.* **17**, 258-265. doi:10.1097/MNH.0b013e3282f9b1a5
- Hu, M. C., Wasserman, D., Hartwig, S. and Rosenblum, N. D. (2004). p38MAPK acts in the BMP7-dependent stimulatory pathway during epithelial cell morphogenesis and is regulated by Smad1. *J. Biol. Chem.* **279**, 12051-12059. doi:10.1074/jbc.M310526200
- Kann, M., Bae, E., Lenz, M. O., Li, L., Trannguyen, B., Schumacher, V. A., Taglienti, M. E., Bordeianou, L., Hartwig, S., Rinschen, M. M. et al. (2015). WT1 targets Gas1 to maintain nephron progenitor cells by modulating FGF signals. *Development* **142**, 1254-1266. doi:10.1242/dev.119735
- Kazama, I., Mahoney, Z., Miner, J. H., Graf, D., Economides, A. N. and Kreidberg, J. A. (2008). Podocyte-derived BMP7 is critical for nephron development. *J. Am. Soc. Nephrol.* **19**, 2181-2191. doi:10.1681/ASN.2007111212
- Kobayashi, A., Valerius, M. T., Mugford, J. W., Carroll, T. J., Self, M., Oliver, G. and McMahon, A. P. (2008). Six2 defines and regulates a multipotent self-renewing nephron progenitor population throughout mammalian kidney development. *Cell Stem Cell* **3**, 169-181. doi:10.1016/j.stem.2008.05.020
- Kopan, R., Chen, S. and Little, M. (2014). Nephron progenitor cells: shifting the balance of self-renewal and differentiation. *Curr. Top. Dev. Biol.* **107**, 293-331. doi:10.1016/B978-0-12-416022-4.00011-1
- Little, M., Holmes, G. and Walsh, P. (1999). WT1: what has the last decade told us? *BioEssays* **21**, 191-202. doi:10.1002/(SICI)1521-1878(199903)21:3<191::AID-BIES3>3.0.CO;2-8
- Luo, G., Hofmann, C., Bronckers, A. L., Sohocki, M., Bradley, A. and Karsenty, G. (1995). BMP-7 is an inducer of nephrogenesis, and is also required for eye development and skeletal patterning. *Genes Dev.* **9**, 2808-2820. doi:10.1101/gad.9.22.2808
- Oxburgh, L., Brown, A. C., Fetting, J. and Hill, B. (2011). BMP signaling in the nephron progenitor niche. *Pediatr. Nephrol.* **26**, 1491-1497. doi:10.1007/s00467-011-1819-8
- Oxburgh, L. and Robertson, E. J. (2002). Dynamic regulation of Smad expression during mesenchyme to epithelium transition in the metanephric kidney. *Mech. Dev.* **112**, 207-211. doi:10.1016/S0925-4773(01)00648-7
- Park, S. H. and Chi, J. G. (1993). Oligomeganephronia associated with 4p deletion type chromosomal anomaly. *Pediatr. Pathol.* **13**, 731-740. doi:10.3109/15513819309048260
- Ryan, D., Sutherland, M. R., Flores, T. J., Kent, A. L., Dahlstrom, J. E., Puelles, V. G., Bertram, J. F., McMahon, A. P., Little, M. H., Moore, L. et al. (2018). Development of the human fetal kidney from mid to late gestation in male and female infants. *EBioMedicine* **27**, 275-283. doi:10.1016/j.ebiom.2017.12.016

- Salomon, R., Tellier, A.-L., Attie-Bitach, T., Amiel, J., Vekemans, M., Lyonnet, S., Dureau, P., Niaudet, P., Gubler, M. C. and Broyer, M. (2001). PAX2 mutations in oligomeganephronia. *Kidney Int.* **59**, 457-462. doi:10.1046/j.1523-1755.2001.059002457.x
- Short, K. M., Combes, A. N., Lefevre, J., Ju, A. L., Georgas, K. M., Lamberton, T., Cairncross, O., Rumballe, B. A., McMahon, A. P., Hamilton, N. A. et al. (2014). Global quantification of tissue dynamics in the developing mouse kidney. *Dev. Cell* **29**, 188-202. doi:10.1016/j.devcel.2014.02.017
- Stark, K., Vainio, S., Vassileva, G. and McMahon, A. P. (1994). Epithelial transformation of metanephric mesenchyme in the developing kidney regulated by Wnt-4. *Nature* **372**, 679-683. doi:10.1038/372679a0
- Wetzel, P., Haag, J., Campean, V., Goldschmeding, R., Atalla, A., Amann, K. and Aigner, T. (2006). Bone morphogenetic protein-7 expression and activity in the human adult normal kidney is predominantly localized to the distal nephron. *Kidney Int.* **70**, 717-723. doi:10.1038/sj.ki.5001653
- Zhang, Y. E. (2017). Non-smad signaling pathways of the TGF- $\beta$  family. *Cold Spring Harb. Perspect. Biol.* **9**. a022129. doi:10.1101/cshperspect.a022129
- Zouvelou, V., Passa, O., Segklia, K., Tsalavos, S., Valenzuela, D. M., Economides, A. N. and Graf, D. (2009). Generation and functional characterization of mice with a conditional BMP7 allele. *Int. J. Dev. Biol.* **53**, 597-603. doi:10.1387/ijdb.082648vz

Supplementary Figure 1

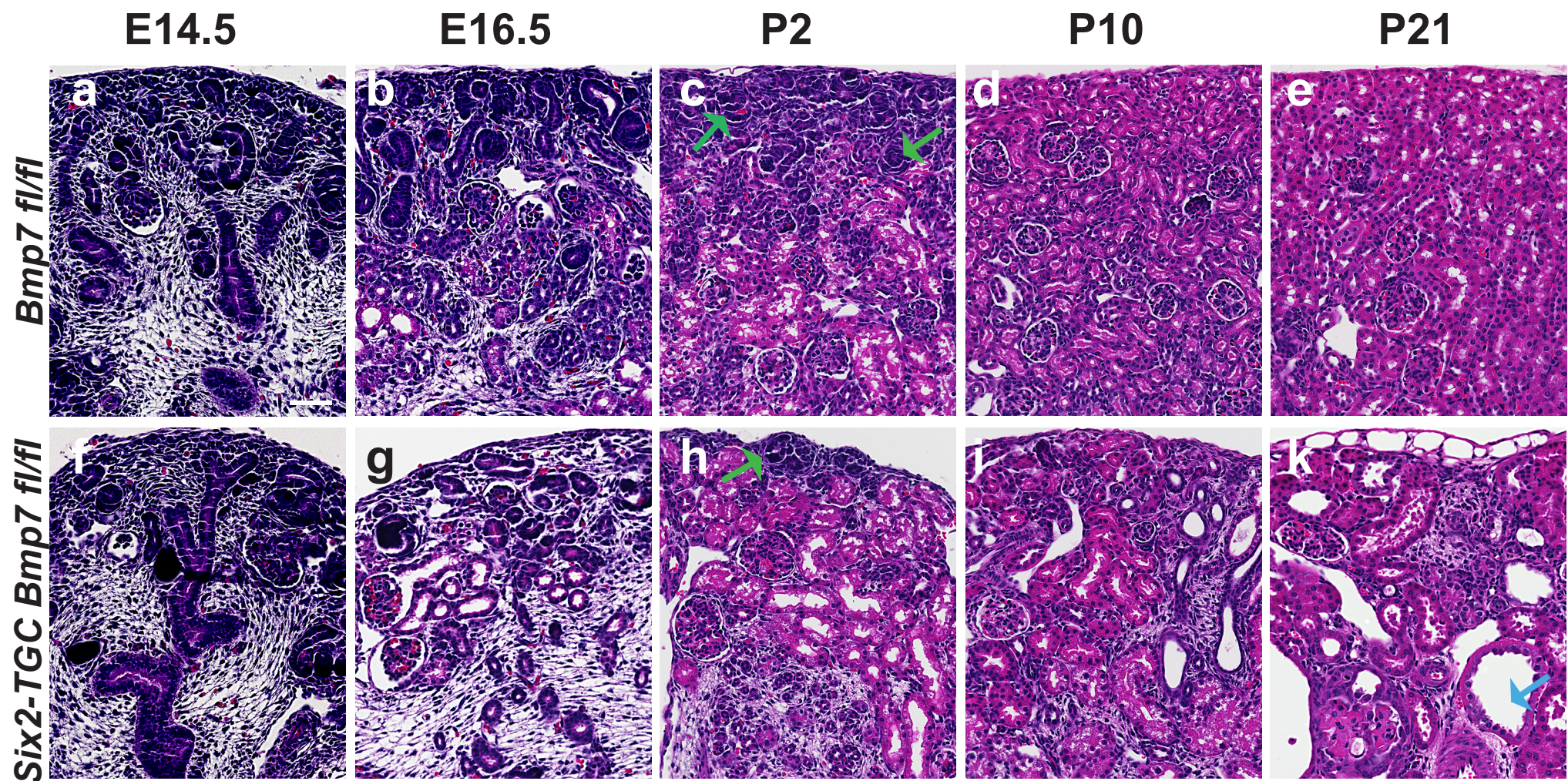


**Fig. S1. Histology of *Bmp7* mutant kidneys** Hematoxylin and Eosin stained sections, all panels at the same scale. (a-e): controls; (f-k) *Bmp7* mutants. Postnatal day time point at the top of each column. Green arrows: S-shaped tubule in (c), immature differentiating structure in (h). Cystic tubule; blue arrow in (k). Scale bar 50  $\mu$ m. All images are representative of three biological replicates.

Supplementary Figure 2

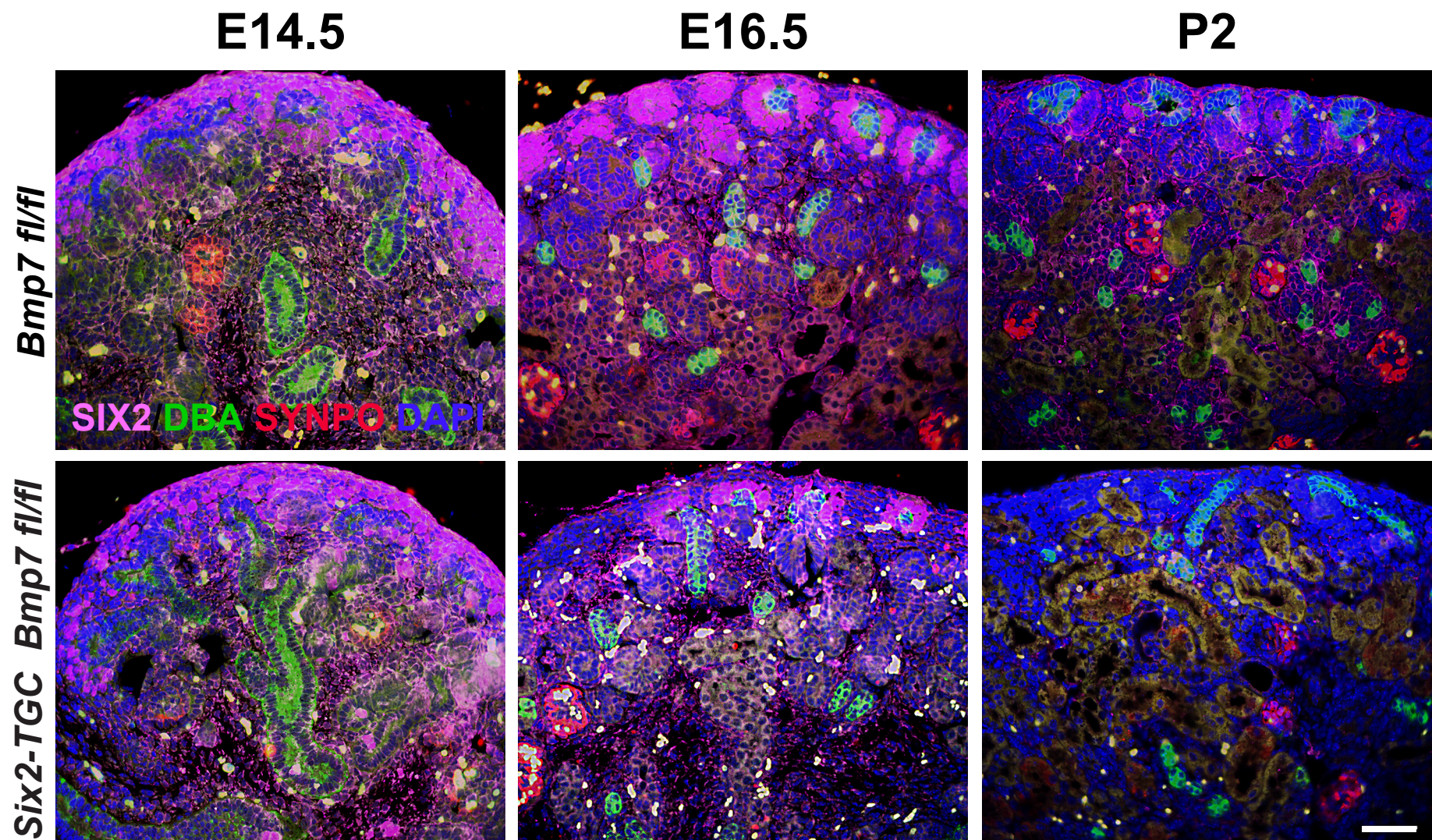


**Fig. S2.** Higher magnification images of time points shown in Figure 1 Scale bar = 50µm. All images are at the same scale. Time points at top of each column, genotypes at left of each row. Pink: Six2, Green: DBA lectin, Red: Synaptopodin. The olive-green color in the E16.5 and P2 panels is autofluorescence characteristic of kidney tubules in paraffin embedded tissues. All images are representative of three biological replicates.

Supplementary Figure 3

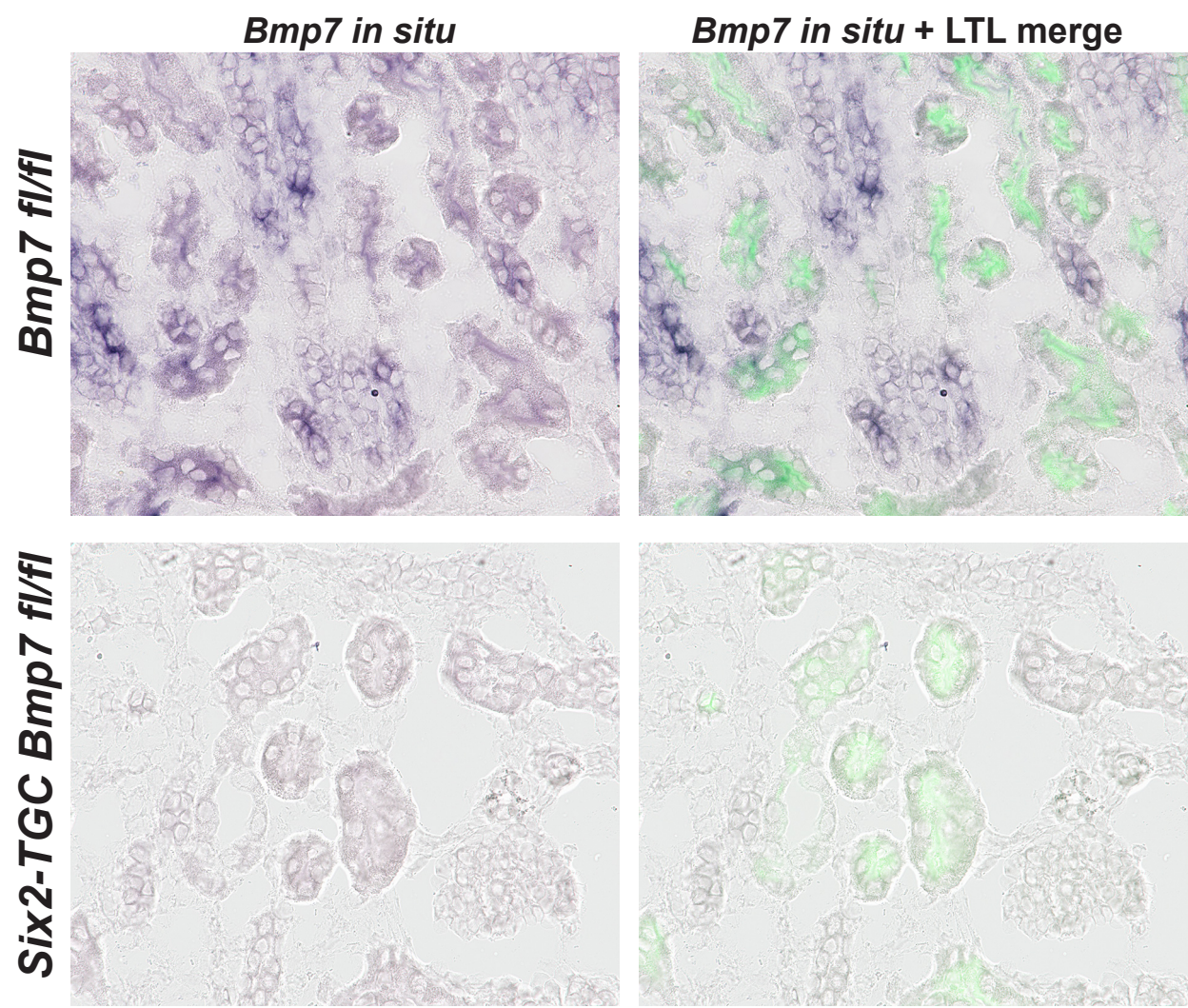


**Fig. S3. Co-imaging of Bmp7 mRNA and LTL lectin.** The Left column shows Bmp7 mRNA only. The right column shows a merge of the in situ hybridization and the LTL-lectin stain (green).

Supplementary figure 4

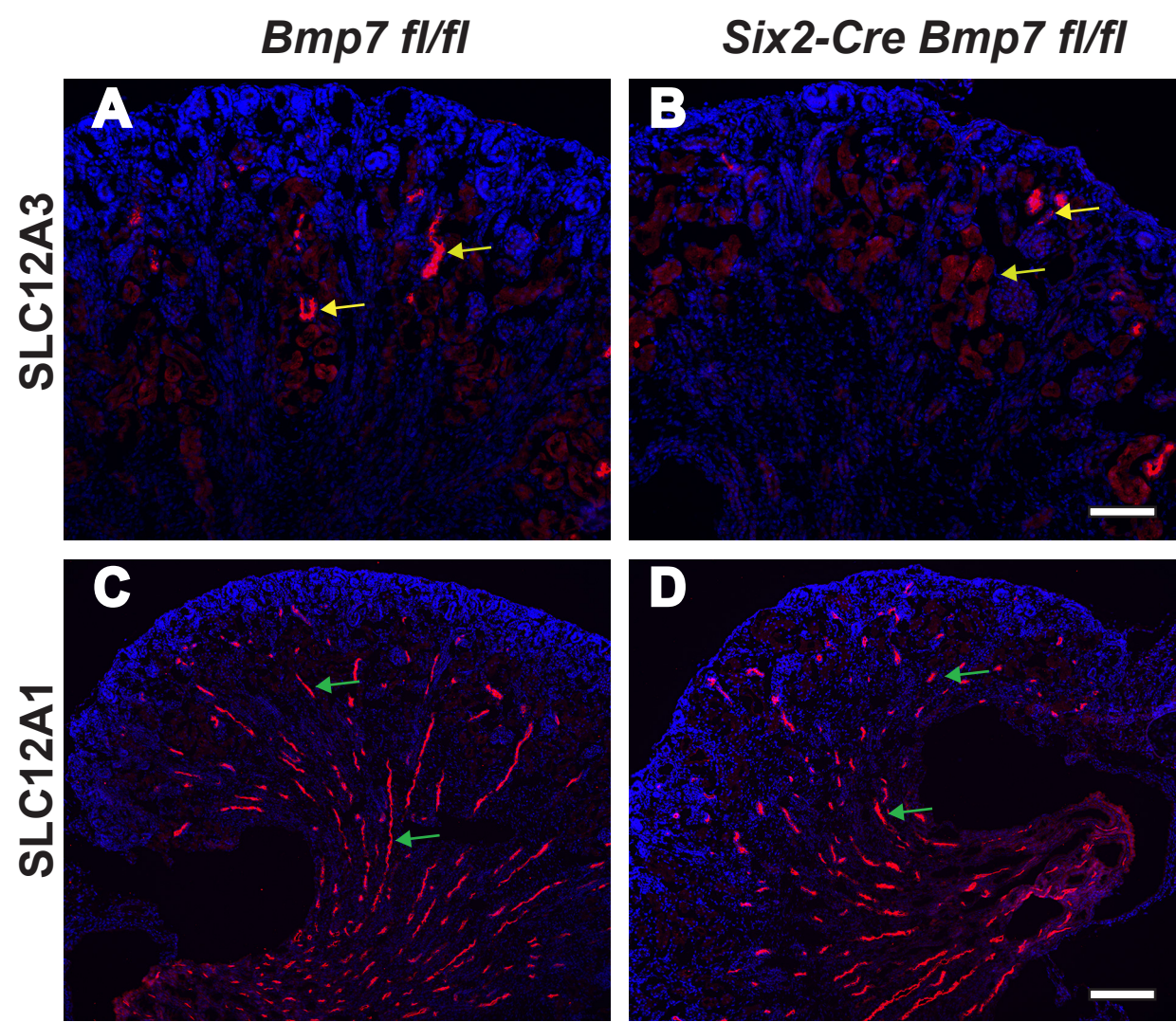


**Fig. S4. SLC12A3 and SLC12A1 staining.** (A,C) controls, (B,D) *Bmp7* mutants. (A,B) SLC12A3 staining for distal tubules (yellow arrows). (C,D) SLC12A1 staining for loops of Henle (green arrows). (A,B) scale bar 100µm; (C,D) scale bar 250µm. All images are representative of three biological replicates.

Supplementary figure 5

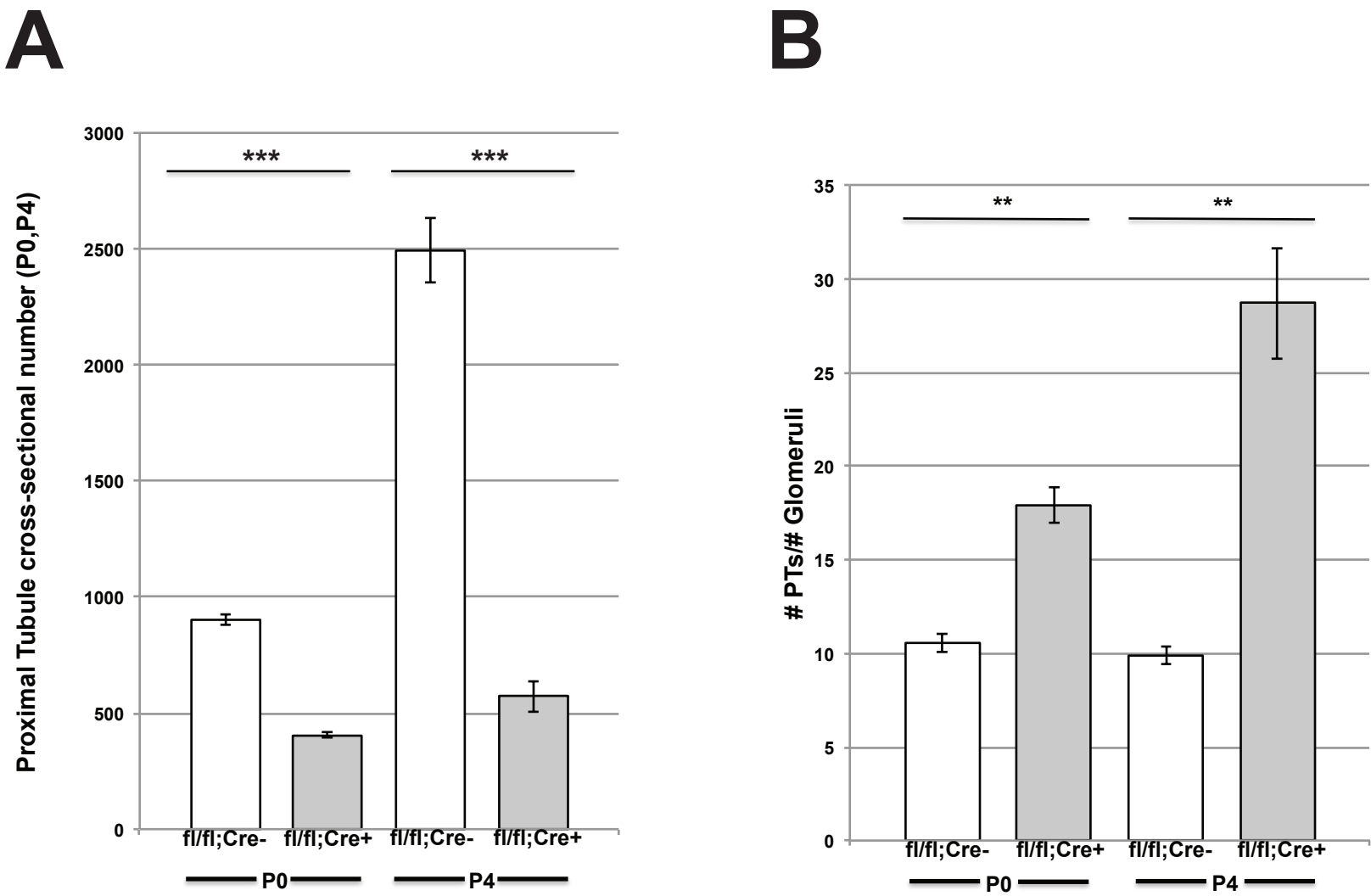


**Fig. S5. Quantification of proximal tubule cross sections.** (A) LTL stained cross sections in P0 and P4 kidneys. Genotypes at bottom of graph. (B) LTL-stained cross sections per glomerulus. All images are representative of three biological replicates.

Supplementary Figure 6

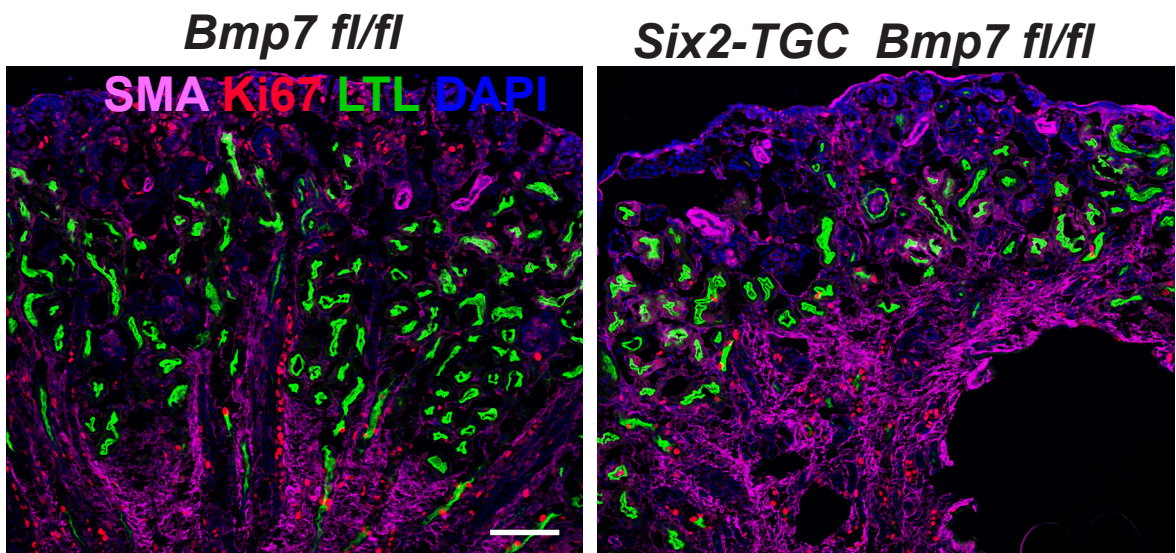


**Fig. S6. SMA and Ki67 immunofluorescence.** Genotypes at the top of each panel. Images are from P2 kidneys. Red: Ki67, Pink: SMA, Green: LTL lectin, Blue DAPI. Scale bar 100  $\mu$ m. All images are representative of three biological replicates.